Individual Blade Control of a 5-bladed Rotor Using the Multiple Swashplate System

Philip Küfmann
philip.kuefmann@dlr.de
project leader

Rainer Bartels
rainer.bartels@dlr.de
research engineer

Berend G. van der Wall
berend.vanderwall@dlr.de
senior scientist

Oliver Schneider
oliver.schneider@dlr.de
research engineer

German Aerospace Center (DLR), Institute of Flight Systems, Braunschweig, Germany

Hermann Holthusen
hermann.holthusen@dnw.aero
project aerodynamicist

Jos Postma
jos.postma@dnw.aero
R&D engineer

German-Dutch Wind Tunnels (DNW), Marknesse, Netherlands

Abstract

After its first wind tunnel test in 2015, the multiple swashplate system (META) as well as the DLR's rotor test rig were modified and upgraded extensively to allow IBC operation on a five-bladed rotor system. In late 2016 a second wind tunnel test was performed on a Mach-scaled, five-bladed model rotor with the goal to reduce vibration, noise and required rotor power on a five-bladed rotor in different flight conditions using proven IBC strategies. Highlights of the test matrix were 2/rev sweeps and the test of different localized pitch control (LPC) strategies for reduction of noise and required rotor power. In simulated high-speed flight, the required rotor power was successfully reduced using a 2/rev input with an amplitude of $1°$. In descent flight condition, significant BVI noise reductions relative to the baseline case were achieved on both sides of the rotor disk through the application of 2/rev HHC as well as a localized pitch control (LPC) schedule. In addition the 5/rev hub vibration levels were reduced significantly both through the application of 3/rev IBC and a vibration controller using a 4-6/rev multi-harmonic IBC signal. The highest reduction was achieved for the vertical 5/rev force, nearby eliminating the most prominent component of rotor hub vibrations

Notation

C_T	thrust coefficient
$F_{x,y,z}$	hub forces (non-rotating frame)
$I_{BM,5}$	index for blade bending moments with influence on 5/rev hub loads
$M_{x,y,z}$	hub moments (non-rotating frame), Nm
N_b	number of blades
p	pressure, kPa
r	radial coordinate, m
R	rotor radius, m
VI_5	weighted 5/rev vibration intrusion index
$y_{tip,el}$	elastic lag displacement at the blade tip
$z_{tip,el}$	elastic flap displacement at the blade tip
α_S	rotor shaft angle, deg
β_{PC}	pre-cone angle
γ	flight path angle of the model, deg
$\Theta_{0,C,S}$	collective and cyclic control angles, deg
Θ_n	n/rev HHC amplitude, deg
σ	solidity
ϕ_n	phase of elastic n/rev blade torsion, deg
φ_n	n/rev HHC phase, deg
ϑ	individual blade pitch angle, deg
μ	advance ratio
ψ	azimuth angle, deg
Ω_{ref}	rotor rotational frequency, rad/s, Hz

Abbreviations

ADC	Analog-Digital Converter
BL	Baseline
DLR	Deutsches Zentrum für Luft- und Raumfahrt e.V. (German Aerospace Center)
DNW	Deutsch-Niederländischer Windkanal (German-Dutch Wind Tunnels)
FTK	Fortschrittliche Taumelscheibenkonzepte (advanced swashplate-concepts)
HART	HHC Aeroacoustics Rotor Test
HHC	Higher Harmonic Control
h.p.	High-Pass filtered
IBC	Individual Blade Control
LLF	Large Low-Speed Facility
LPC	Localized Pitch Control
META	MEhrfach-TAumelscheibe (Multiple Swashplate Control System)
MN, MV	Minimum Noise, Minimum Vibration
SKAT	Skalierung und Risikominimierung von Technologie bei innovativem Design (Scaling and risk-minimization for technology with innovative design)
SPL	Sound Pressure Level
SPL.rel	Sound Pressure Level relative to max. level of the respective frequency range
SPR	Stereo Pattern Recognition

1. Introduction

Helicopters, while having advantages making them indispensable in many applications, are prone to high noise and vibration levels as well as comparatively high power consumption in high-speed flight. In addition to passive measures – such as optimized fuselage and rotor blade designs – the field of active rotor control offers a variety of approaches to address these specific problems directly at their source [1–3], many of which have been the subject of research at DLR [4–7]. In 2008, the DLR introduced and patented a novel active rotor control system for achieving complete individual blade control (IBC) on rotors with more than three blades without using actuators in the rotating frame [8–11]. The Multiple Swashplate System (META) has since been integrated into the DLR's rotor test rig and its IBC capabilities have been successfully demonstrated on a four-bladed rotor both in hover conditions [12] and in the wind tunnel [13, 14] within the project FTK-META.

As part of the follow-up project SKAT (scalability and risk-minimization of technology with innovative design) together with Airbus Helicopter Germany, the Multiple Swashplate System and the DLR's rotor test rig have since been equipped with a five-bladed rotor hub and modified for 5-blade IBC operation. After extensive updates to both soft- and hardware and pre-tests at DLR's own rotor test facility, the system entered the DNW's large low speed facility (LLF) in the Netherlands for nine days of testing. The goal of this wind tunnel test was to research the transferability of established IBC strategies for performance enhancement as well as noise and vibration reduction from a four-bladed to a five-bladed rotor system.

The first part of this paper outlines the changes and updates of the META system, the test setup and the measurement systems used in the wind tunnel. The second part of the paper then discusses selected results of the wind tunnel test with regards to changes in noise emissions, vibration levels and rotor performance and in comparison to results from the earlier FTK-META test.

2. Test setup

2.1. Text conditions and test matrix

In order to maintain comparability between the results, the test hardware as well as the principal test conditions and procedures closely resembled those of the first wind tunnel test of the META system in the project FTK-META, which are extensively documented in [13] and [14]. The following section therefore only outlines the changes and upgrades made for accurate and safe 5-blade IBC operation of the META system as well as changes in the measurement setup at the DNW LLF.

As in the FTK-META test, IBC tests were performed for three different simulated flight conditions – descent flight, cruise and high-speed level flight. The respective trim conditions are summarized in table 1.

Table 1: Forward flight trim conditions overview

Condition	$V_\infty, m/s$	$100 \cdot C_T$	γ	α_S
Descent	33	0.600	7.0°	+6.7°
Cruise	66	0.604	0.0°	−5.6°
High-speed	76	0.605	0.0°	−7.5°

Besides single frequency HHC with frequencies from 2/rev to 6/rev, multi-harmonic control inputs were tested using a T-matrix based vibration control algorithm. Based on random multi-harmonic inputs and measured 5/rev vibrations, this algorithm first identifies a linear model of the rotor (the so called T-matrix) and subsequently uses a quadratic programming approach to determine optimized HHC signals for vibration reduction while adhering to user-set limits. The details of the control algorithm are documented in [15]. Additionally, the effects of localized pitch control inputs which have been shown to be potentially beneficial for BVI-noise reduction [16] and rotor performance enhancement [17–20], were evaluated. An overview of the test matrix is given in table 2.

Table 2: Test matrix overview

IBC input / phase sweeps	$V_\infty, m/s$ 33	66	76
2/rev HHC $\Theta_2 = 0.4°$	✓		
2/rev HHC $\Theta_2 = 0.8°$, $\Theta_2 = 1.0°$		✓	✓
3/rev $\Theta_3 = 0.3°$	✓		
3/rev $\Theta_3 = 0.5°$, $\Theta_2 = 0.8°$		✓	✓
4/rev $\Theta_4 = 0.2°$	✓	✓	✓
4/rev $\Theta_4 = 0.4°$	✓		✓
4/rev $\Theta_4 = 0.55°$	✓	✓	
5/rev $\Theta_5 = 0.2°$	✓		✓
5/rev $\Theta_5 = 0.35°$	✓	✓	✓
5/rev $\Theta_5 = 0.45°$	✓	✓	
6/rev $\Theta_6 = 0.2°$	✓		✓
6/rev $\Theta_6 = 0.3°$	✓	✓	✓
6/rev $\Theta_6 = 0.4°$	✓	✓	
Vibration control 4-6/rev	✓	✓	✓
LPC $\Theta_{dip} = \pm0.3°$, $\Theta_{dip} = \pm0.6°$	✓	✓	
LPC $\Theta_{dip} = \pm0.75°$	✓	✓	✓
LPC $\Theta_{dip} = \pm1.1°$		✓	✓

The LPC function tested in the wind tunnel consists of one so-called 'dip', which increases or decreases the pitch angle of the rotor blade in a certain, predefined sector of the rotor disk. To make a realization of this kind of control signal possible with the META system,

the change in pitch was not defined as a step function, but as a function with a semi-sinusoidal lead-in and lead-out. The details regarding the definition of the LPC-function can be found in [20].

Both the amplitude Θ_{dip} and the azimuthal location (or phase) φ_{dip} were modified during the LPC-tests documented in this paper. The width of the LPC functions remained constant at $90°$ with a symmetrical lead-in and lead-out ($\Phi_1 = \Phi_2 = 45°$) and no plateau ($\Phi_H = 0°$). An example of the tested LPC function with a pitch increase of $\Delta\vartheta_{LPC} = 0.75°$ at the azimuthal position $\varphi_{dip} = 90°$ is shown in Fig. 1.
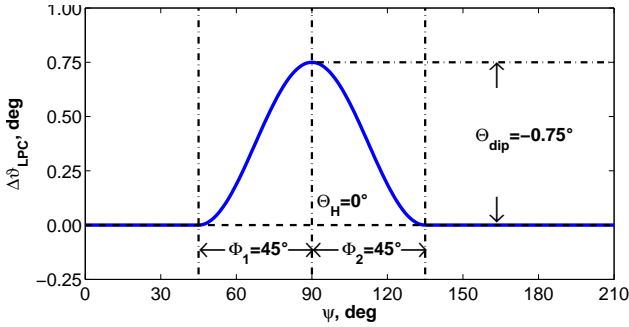
Figure 1: Basic form of LPC-function (dip)

2.2. Model rotor and META

In order to support IBC operation with 5 blades, the DLR's rotor test rig was equipped with a five-bladed rotor hub designed on the basis of the preexisting Bo105 model rotor hub, see Fig. 2.
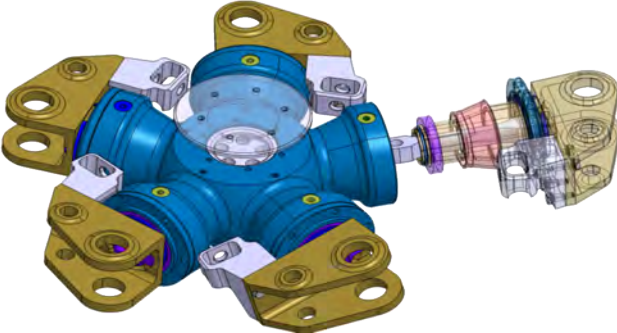
Figure 2: CAD-drawing of 5-bladed Bo105-type hub

Furthermore, the multiple swashplate system originally designed for 4-bladed model rotors was modified in both hard- and software. Both swashplates were redesigned to accommodate a fifth control rod, resulting in an asymmetric distribution of control rods on the swashplates. The rotor is split up into two independent subrotors with 2 blades on the outer swashplate and 3 blades on the inner swashplate. A schematic depiction of the META's two subrotors for five-bladed operation is shown in Fig. 3.

The META's control software for IBC and LPC-operation was modified accordingly. Due to the asym-
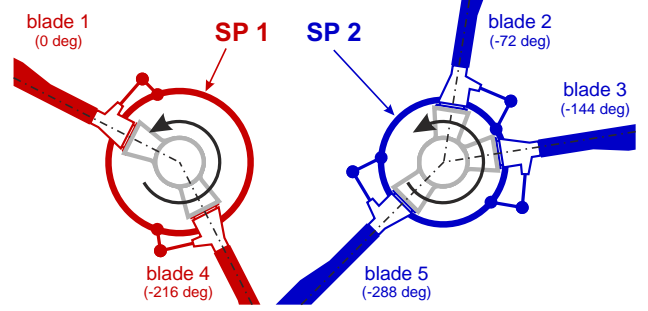

Figure 3: Subrotors of the 5-bladed META system

metric arrangement of rotor blades on the respective swashplates, 2/rev and 3/rev control in the rotating frame result in multi-frequency control signals for the actuators in the non-rotating frame. Besides limiting control authority for these frequencies, this made the control system much more susceptible to small differences in the dynamic behaviour of the hydraulic actuators themselves as well as signal runtime differences between actuators, resulting in inacceptably high blade-to-blade differences in both amplitude and phase of HHC signals.

As a remedy, the controller for the META's hydraulic actuators was upgraded to a notch-filter based system and the rotor hub was equipped with redundant pitch angle sensors (2 per blade). On top of the acuator strokes computed in real time using a kinematic model, the signals from the pitch angle sensors are fed back into a PI-controller with limited autority to ensure the correct IBC amplitude and phase for each blade. With the upgraded control system, control signal deviations and blade-to-blade differences were effectively reduced to $\Delta\Theta_n \leq 0.05°$ in amplitude and $\Delta\varphi_n \leq 1°$ in phase for each frequency.

The resulting control frequencies for the actuators of the 5-bladed META system for each n/rev HHC input (2-6/rev) are summarized in table 3.

Table 3: Control modes on 5-bladed META system

IBC input	Actuator control frequencies				
	1/rev	2/rev	3/rev	4/rev	5/rev
2/rev	✓	✓	✓		
3/rev		✓	✓	✓	
4/rev					✓
5/rev					✓
6/rev					✓

2.3. Measurement equipment

The measurement equipment and the measurement procedures were mostly identical to the FKT-test as documented in [13,14]. The following sections therefore contain only a short description of the measure-

ments systems, as well as upgrades and deviations from the FTK-setup.

2.3.1. Acoustics

The microphone systems used to measure the acoustic characteristic of the SKAT rotor are practically identical to the setup which was applied for the META test in 2016 [13]. Both systems and their position relative to the wind tunnel model are shown in Fig. 4.
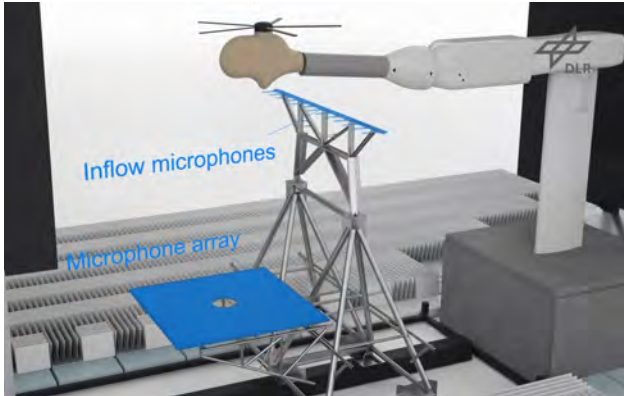

Figure 4: Wind tunnel model and acoustic systems

With the first system the flyover noise field below the rotor plane was measured in order to produce so called 'noise-carpet' plots. The system consists of 13 microphones installed on a traversable in-flow wing. The microphone signals were measured in parallel by two of DNW's 16bit-ADC Viper acquisition systems. One data set of signals was measured in phase-locked mode with 2048 acquisition steps per rotor revolution and the other data set was measured with a fixed sampling frequency of $102.4\ kHz$. For both acquisition types the continuous sampling duration was at least $10\ s$ ($\approx$175 rotor revolutions).

The second acoustic system with a phased microphone array of $4x4\ m^2$ aperture and 140 microphones was used for noise source localization within the rotor disk. The array was placed out-of the flow onto the traverse support for the in-flow microphones of the first acoustic system. The signals from the array were measured with DNW's 24bit-ADC Viper HDR system with a fixed sampling frequency of $102.4\ kHz$ and a sampling duration of at least $10\ s$.

2.3.2. SPR-system

The same SPR-system as in the FTK-test [13] was used for stereoscopic tracking of blade-mounted markers and to determine the contribution of the individual modes in flapping, lead-lag, and torsion after post-processing.

The markers were detected at 30 equally spaced azimuthal positions and the number of averaged samples to determine the final marker positions was reduced from 10 (FTK-project) to 5, which proved sufficient in terms of tracking accuracy while reducing acquistion times considerably. Twelve strobe lights were mounted on a ring-shaped truss illuminating the rotor from above with light pulses of $0.5\ \mu s$ duration. The cameras were equipped with band pass filters to pass only the fluorescence light and block out stray light interfering with the measurement, thus ensuring good contrast of the markers detected in the images.

To obtain optical pitch angle measurements (see also 'Blade deformations' section), two additional markers per blade were applied to the aluminum blade mounting bracket, directly adjacent to the two resistive pitch angle sensors mounted on the pitch arms of rotor hub. Fig. 5 shows the different marker positions on the wind tunnel model mounted in the test section of the DNW LLF.
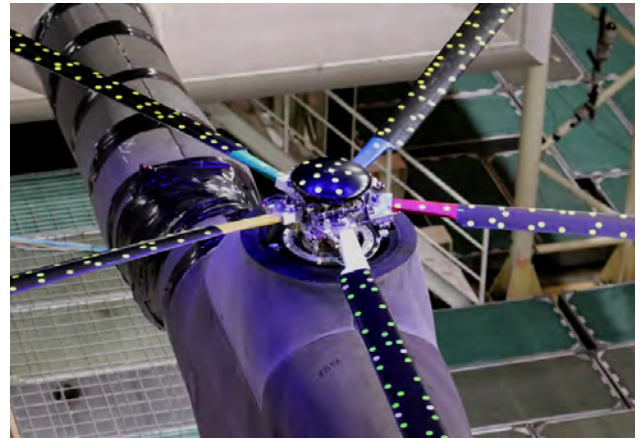

Figure 5: Marker positions on model rotor blades, blade roots and rotor hub

2.3.3. Blade instrumentation

For this wind tunnel test, the FTK-blades from the first wind tunnel test [13, 14] were re-used. In addition, a fifth FTK-blade was manufactured and equipped with several dynamic pressure sensors for the detection of BVI-events. The positions of the pressure sensors on the 5th FTK-blade are shown in Fig. 6.
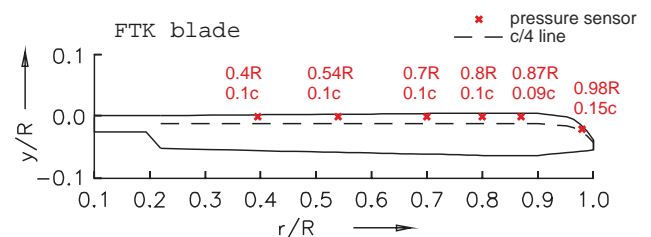

Figure 6: Pressure sensor positions on 5th FTK-blade

2.4. Test procedure

In general the test procedure as well as the procedures for SPR blade tracking and acoustic measurements were identical to the procedures applied during the FTK-test. Details on the test and measurement procedures as well as the applied post-processing techniques can be found in [13].

The model rotor was manually trimmed for zero hub moments ($M_X \stackrel{!}{=} M_Y \stackrel{!}{=} 0$) and the respective thrust level for the chosen flight condition. If IBC was applied, the model was retrimmed before measuring and taking a datapoint.

For acoustic measurements, the microphone array system was used to quickly and efficiently determine maximum and minimum BVI-noise cases as well as the noise source locations within the rotor disk. In a second step, measurements with the microphone traverse were taken for specific test cases which were selected based on the results from the array system. In addition, online results of the blade pressure measurements were used to verify the validity of the array results for the determination of the specific test point parameters.

2.5. Power corrections

Due to the dynamic behaviour of the wind tunnel model slight changes of thrust, propulsive force and hub moments occured and their effects on the measured, effective rotor power P_{eff} had to be corrected during post-processing, as outlined in [13]. During the wind tunnel test with a five-bladed rotor system, additional trim measurements were obtained to determine the effect of hub moment changes ($M_X \neq 0$, $M_Y \neq 0$) on the effective rotor power P_{eff}. As a result, a correction based on changes in hub moments was added:

$$(1) \qquad \Delta P_M = c_x \cdot M_X + c_y \cdot M_Y$$

The coefficients c_x and c_y were determined from additional trim measurements by applying the method of least squares:

$$(2) \quad \begin{aligned} c_x &= \frac{-\sum M_Y^2 \cdot \sum M_X \Delta P + \sum M_X M_Y \cdot \sum M_Y \Delta P}{\sum M_X^2 \cdot \sum M_Y^2} \\ c_y &= \frac{-\sum M_X^2 \cdot \sum M_Y \Delta P + \sum M_X M_Y \cdot \sum M_X \Delta P}{\sum M_X^2 \cdot \sum M_Y^2} \end{aligned}$$

However, compared to the power corrections due to changes in thrust and propulsive force, ΔP_M was found to be negligible. As a result, measurements from FTK-META remain comparable to those obtained with the 5-bladed rotor system.

3. Results

3.1. Rotor performance

Several HHC inputs were tested for rotor performance enhancement, with 2/rev being the most effective approach. Fig. 8 shows the change in effective rotor power P_{eff} over the 2/rev phase input in high-speed flight condition ($\mu = 0.345$) or different values of Θ_2.
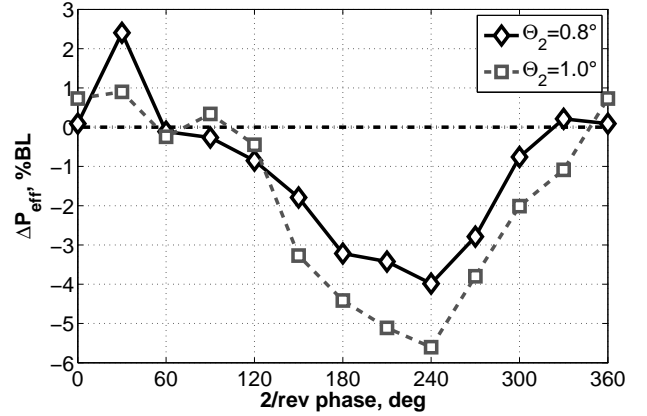

Figure 7: Change of P_{eff} during 2/rev phase sweep

With 2/rev HHC, the maximum reduction in effective rotor power of $\Delta P_{eff} = -5.6\%$ was measured for an amplitude of $\Theta_2 = 1.0°$ at a phase setting of $\varphi_2 = 240°$. Both curves covering the phase sweeps for the respective amplitudes are near sinusoidal. The optimum phase angle corresponds well with results from the FTK-META-WK test, where the maximum power reductions using 2/rev HHC were found for phase angles of $184° \leq \varphi_2 \leq 244°$ [13, 14]. The increase of the measured power reduction with Θ_2 suggests that even higher power savings can be reached with higher 2/rev amplitudes.

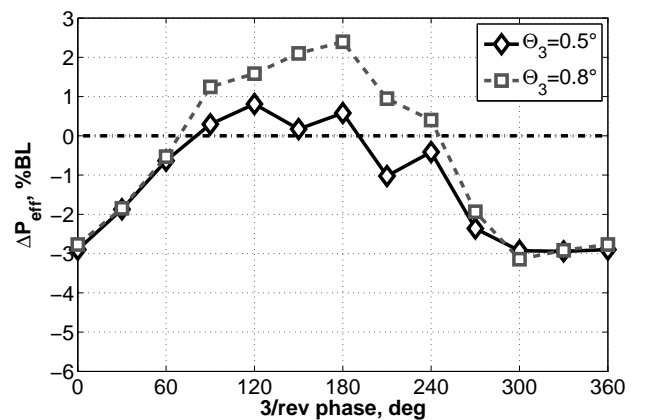The effects of 3/rev HHC on effective rotor power are shown in Fig. 8 for two different amplitudes. Here, the

Figure 8: Change of P_{eff} during 3/rev phase sweep

effective rotor power was reduced by a maximum of $\Delta P_{eff} = -2.8\%$ at zero phase angle ($\varphi_3 = 0$) and

an amplitude of $\Theta_3 = 0.5°$. While a higher 3/rev amplitude seems to lead to a higher power increase for $90° \leq \varphi_3 \leq 210°$, this is not the case for power reductions where a saturation seems to be reached at $\Theta_3 = 0.5°$.

3.2. Vibration reduction

3.2.1. Single frequency phase sweeps

To assess the vibration level of the model a vibration intrusion index VI_5 was defined in accordance with [21, 22] as a weighted combination of 5/rev hub forces and moments using the virtual weight W_0 of the scaled model and rotor radius R to obtain non-dimensional values.

(3)
$$VI_5 = \frac{1}{W_0}\sqrt{(0.5 \cdot F_{X,5})^2 + (0.67 \cdot F_{Y,5})^2 + F_{Z,5}^2} + \frac{1}{R \cdot W_0}\sqrt{M_{X,5}^2 + M_{Y,5}^2}$$

Fig. 9 shows the averaged baseline case vibration index of the five bladed SKAT rotor over the test conditions. The rotor exhibits vibrations which almost linearly increase with the flight speed. At high speed flight (76 m/s, $\mu = 0.345$) the vibration level is about three times higher than in descent flight at 33 m/s ($\mu = 0.15$).
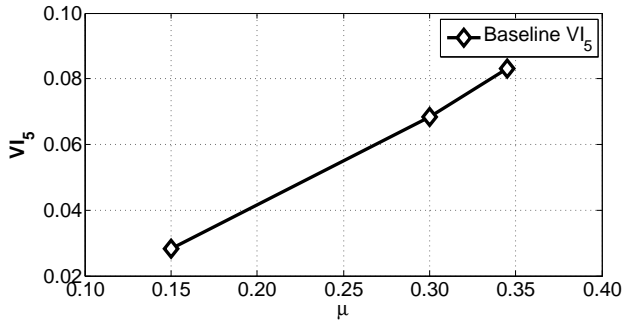
Figure 9: Vibration intrusion index VI_5 at different flight conditions.

3/rev to 6/rev blade pitch inputs with different control amplitudes and phases were tested to analyse the vibration characteristics of the five bladed rotor. For reasons of consistency and comparability of results, the HHC amplitudes for 3/rev and 4/rev HHC were as close as possible to the amplitudes used during the FTK-test [13].

However, the amplitudes for 4/rev to 6/rev HHC (see table 2) proved too high to achieve reductions of the vibration intrusion index VI_5, which was increased at all flight speeds and phase settings for these HHC frequencies. The main reason for this behaviour lies

within the kinematics of the multiple swashplate system. Since 4–6/rev HHC in the rotating frame is realized by (collective and cyclic) 5/rev swashplate movements, the META's hydraulic actuators mounted on the baseplate directly affect the 5/rev forces and moments measured by the rotor balance and offset the value for the intrusion index VI_5 considerably.

In contrast, 3/rev HHC inputs on the 5-bladed rotor system are realized with multicyclic movements of the two swashplates with frequencies between 2/rev and 4/rev. Without the 5/rev actuation forces acting on the rotor balance, 3/rev HHC led to suitable vibration reductions. In the high speed case at $\mu = 0.345$, the vibration level was decreased by 60% with an amplitude of $\Theta_3 = 0.8°$ and a phase angle of $\varphi_3 = 0°$, see Fig. 10.
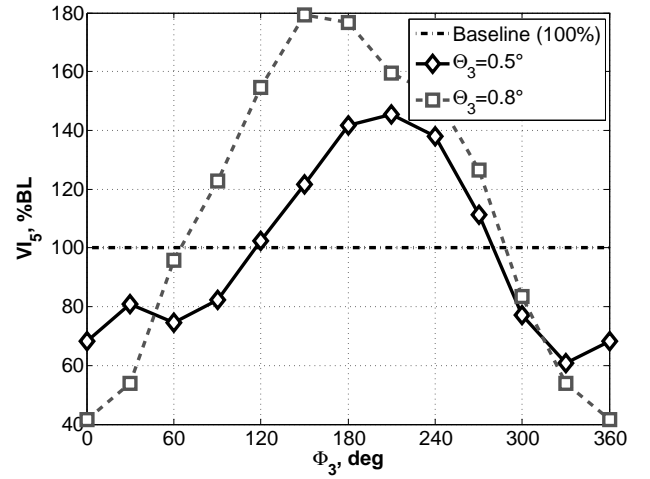
Figure 10: Effect of 3/rev HHC on VI_5 at high speed flight ($\mu = 0.345$).

The highest reduction in effective rotor power had been measured for the same control settings (see Fig. 8), showing the potential of 3/rev HHC for simultaneous performance enhancement and vibration reduction on a 5-bladed rotor system.

In order to make a qualitative assessment of changes in vibration levels possible without the influence of 5/rev actuator forces, a new index was defined using the 4/rev to 6/rev out-of-plane and in-plane blade bending moments from $N_b = 5$ blades, see Eq. (4).

(4)
$$I_{BM,5} = N_b\sqrt{M_{f,5}^2} + \frac{N_b}{2}\sqrt{M_{f,4}^2 + M_{f,6}^2} + \frac{N_b}{2}\sqrt{M_{l,4}^2 + M_{l,6}^2}$$

The corresponding forces in the rotating frame are transformed into 5/rev loads in the non-rotating frame and thus can be used as an indicator for changes in 5/rev vibration levels. For the 3/rev phase sweep,

the curves for $I_{BM,5}$ qualitatively match the curves for the vibration intrusion index VI_5 and the maximum reduction in both cases occurs for an amplitude of $\Theta_3 = 0.8°$ at a phase setting of $\varphi_3 = 0°$, see Fig. 10 and Fig. 11.
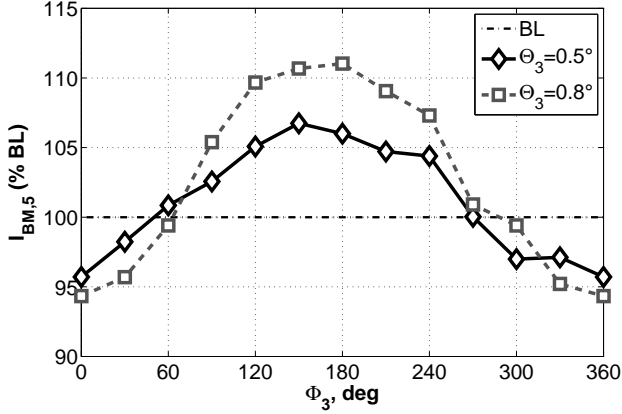

Figure 11: Effect of 3/rev HHC on $I_{BM,5}$ at high speed flight ($\mu = 0.345$).

Fig. 12 shows the development of $I_{BM,5}$ for the 4-6/rev phase sweeps with different amplitudes. With 3/rev control the maximum reduction of $I_{BM,5}$ was measured around 5% and corresponded to a reduction of the vibration intrusion index of $\Delta VI_5 \approx 60\%$. Here, reductions of up to $\Delta I_{BM,5} \approx 12\%$ were reached using a 4/rev input with an amplitude of $\Theta_4 = 0.4°$ at a phase setting of $\varphi_4 = 360°$. Additionally, the maximum reduction of $I_{BM,5}$ occured for phase settings between $\varphi_n = 300°$ and $\varphi_n = 360°$ for all control frequencies from 4/rev to 6/rev.
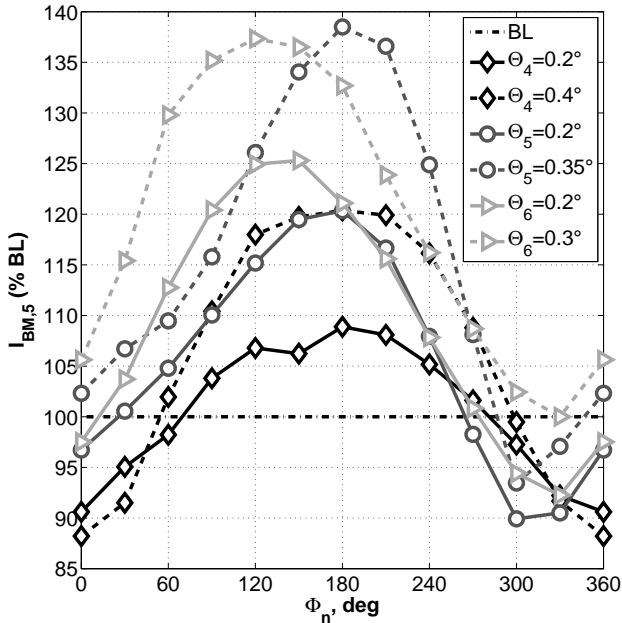

Figure 12: Effect of 4-6/rev HHC on $I_{BM,5}$ at high speed flight ($\mu = 0.345$).

Therefore, when compared to the results of the 3/rev phase sweep, a much higher reduction or even a near complete elimination of 5/rev vibratory hub loads (without taking actuator loads into account) is deemed possible by using single- or multiharmonic control inputs with frequencies of 4-6/rev.

3.2.2. Multi-harmonic vibration control

During the project FTK-META-WK, a vibration control algorithm had been integrated into the META control software [15]. This control algorithm combines the well-known T-matrix contol approach [23] with methods for optimizing control solutions while still adhering to user-set limits (e.g. limits of the used actuation system) [24]. Following the integration process and first tests of the controller on a 4-bladed model rotor in hover conditions, the algorithm was modified for 5-bladed operation, targeting 5/rev hub vibrations using multicyclic 4–6/rev HHC inputs.

The test of this vibration controller in the wind tunnel demonstrated its effectiveness for all test conditions. Depending on the test condition, the controller was able to reduce the vibration intrusion index by up to 83% (high-speed flight), see Fig. 13. Due to the 5/rev actuator forces acting on the rotor balance during 4–6/rev HHC operation, the optimum HHC amplitudes determined by the control algorithm were low compared to the earlier open-loop tests, see table 4.
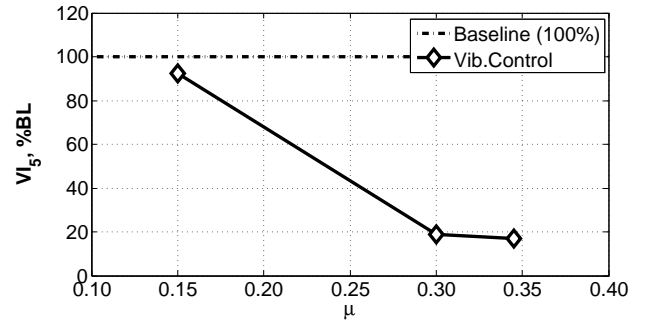

Figure 13: Vibration controller results using 4/rev–6/rev HHC at all tested flight conditions.

Table 4: Vibration controller results

condition	descent 33 m/s	cruise 66 m/s	high-speed 76 m/s
4/rev Θ_4	0.02°	0.0°	0.02°
5/rev Θ_5	0.0°	0.05°	0.05°
6/rev Θ_6	0.04°	0.05°	0.07°
ΔVI_5	7%	81%	83%

Fig. 14 shows the 5/rev magnitudes of the hub forces and moments for the baseline case as well as two

subsequent controller inputs at $76\ m/s$ ($\mu = 0.345$). The first contoller solution ('step 1') reduced mainly the vertical and lateral 5/rev forces ($F_{Z,5}$ and $F_{Y,5}$) while the 5/rev roll moment ($M_{X,5}$) remained nearly unchanged. In a second step, further significant load reductions compared to the first control solution were reached in all axes, and the previously unaffected roll moment $M_{X,5}$ was reduced to 56% of its baseline value. The highest single reduction was achieved for the vertical 5/rev force $F_{Z,5}$ with nearly 93%.
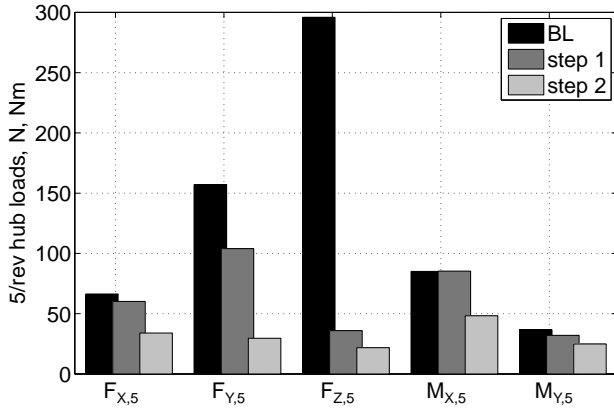
Figure 14: Changes in 5/rev hub loads during vibration controller operation

While the results presented here prove the effectiveness of the control algorithm used, it must be noted that due to the mechanical setup of the META system, a significant portion of the achieved 5/rev vibration reduction was reached due to 5/rev actuator forces counteracting the 5/rev baseline vibrations rather than aerodynamic effects in the rotating frame.

3.3. Noise investigations

3.3.1. Finding the maximum BVI condition

In a first step, the maximum BVI condition in simulated descent flight at $33\ m/s$ was determined by varying the rotor shaft angle α_S and analyzing measurements taken by the microphone array system. Fig. 15 shows the narrow band spectra of the relative sound pressure level (SPL.rel) measured within the rotor plane during the α_S-variation.

As can be seen in Fig. 15, the highest noise level was recorded for a rotor shaft angle of $\alpha_S = 7°$ with the highest overall peak near $630\ Hz$. The maximum BVI case was also confirmed by the analysis of leading edge pressure distributions which was performed in parallel to the microphone array analysis. For this purpose the high frequency content ≥ 10/rev was analyzed for radial sections of 54, 70, 80 and 98% radius within the regions of interest, i.e., the azimuth ranges on advancing side ($30° \leq \psi \leq 90°$) and on the retreating side ($270° \leq \psi \leq 330°$).
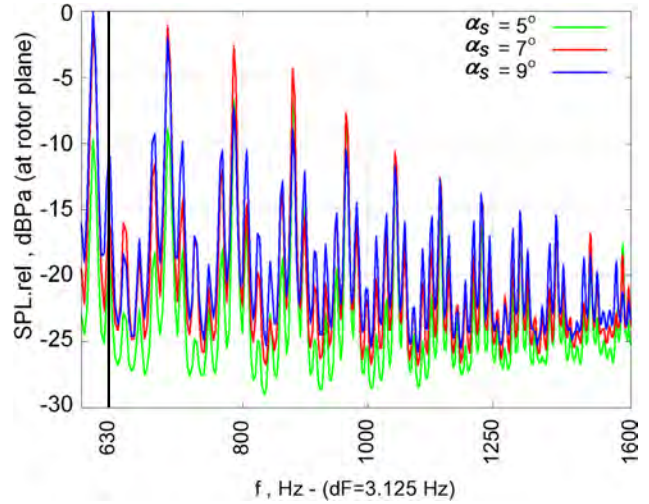

Figure 15: Narrow-band spectra of SPL.rel measured in the rotor plane

Instead of time histories, time derivatives may provide a clearer impression of the BVI-intensity, because the derivative is the physical source of noise radiation. Examples are given in Fig. 16 (adv. side) and Fig. 17 (ret. side) for the identification of the maximum noise case at 33 m/s wind speed for the range of shaft angle $5° \leq \alpha_S \leq 9°$. Those BVI that are most parallel to the blade leading edge are located within the grey shaded area. Large pressure gradients (positive and negative) over a large radial extension (especially at the blade tip where the highest Mach numbers occur) and within the grey shaded areas (representing the blade parallel BVI zones) can be seen as an indicator for strong BVI noise. The strongest events on both the advancing and retreating side can be found at 7° shaft angle of attack.

For the same cases the qualitative contours of BVI locations and their intensity are shown in Fig. 18. The 5° shaft angle (top graph) shows advancing side BVI more upstream (to the left) and the 9° (lower graph) more downstream (to the right) than at 7° (middle graph). The same is found on the retreating side. It is obvious that the shaft angle setting of $\alpha_S = 7°$ is the one with highest BVI intensity and thus the maximum noise radiation condition, which confirms the analysis of microphone array measurements shown before in Fig. 15. Therefore, this case was selected as the baseline (BL) case for all active control parameter variations.
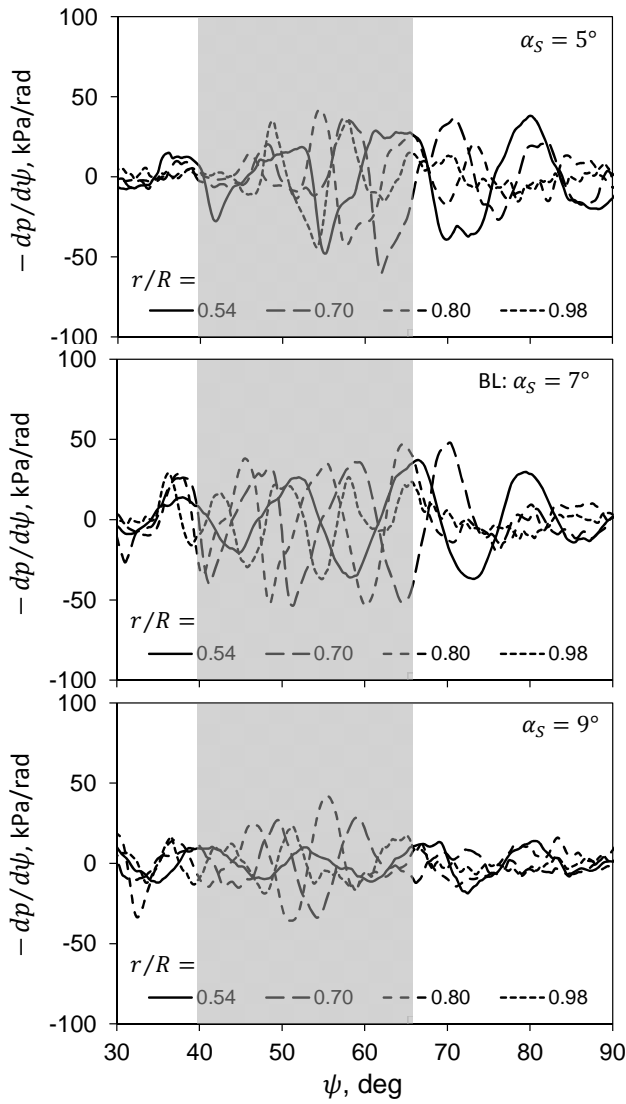
Figure 16: Time derivative of pressure signals during sweep of angle of attack, h.p. filtered at 10/rev, advancing side, $33\ m/s$.
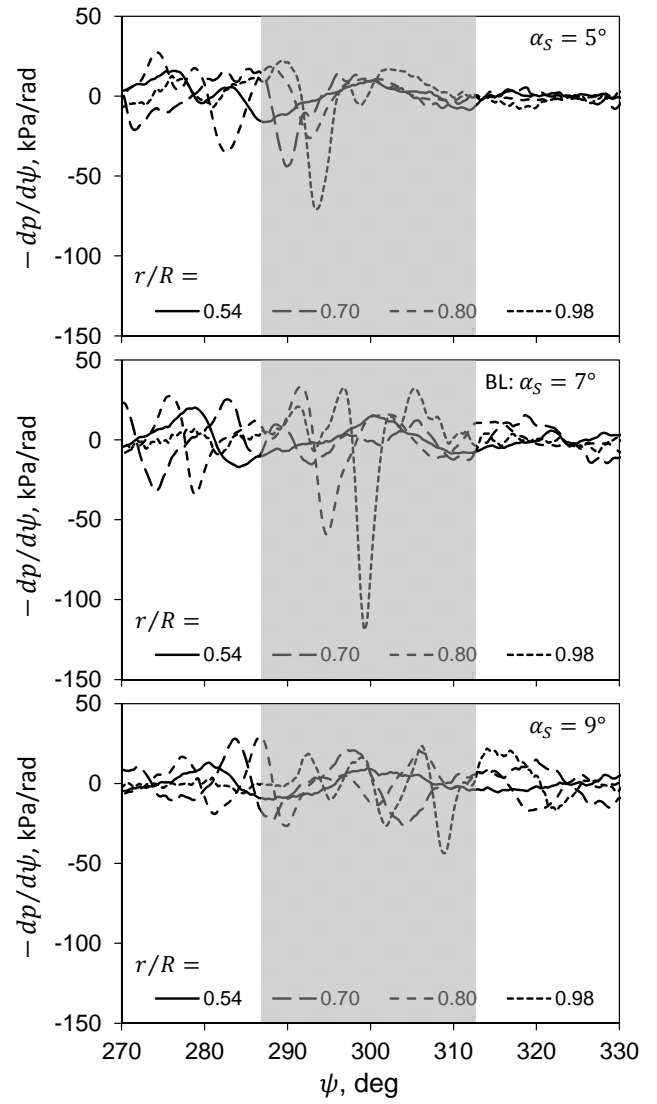
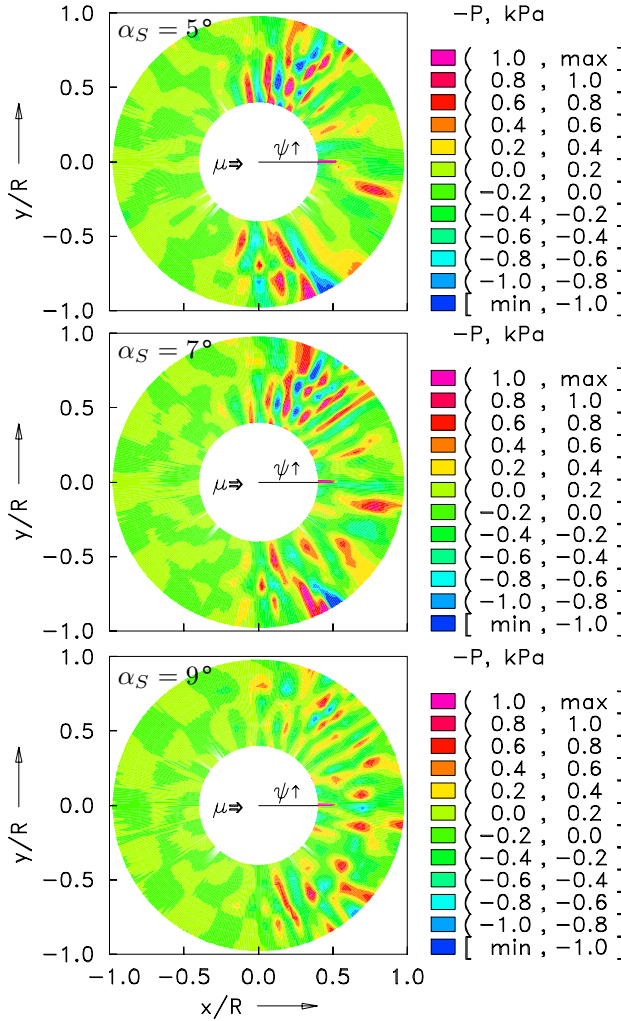Figure 17: Time derivative of pressure signals during sweep of angle of attack, h.p. filtered at 10/rev, retreating side, $33\ m/s$.

Figure 18: BVI in pressure signals during sweep of angle of attack, h.p. filtered at 10/rev, $33\ m/s$.

3.3.2. Noise reduction through HHC and LPC

Once the BL case was defined, HHC phase sweeps at 2 to 6/rev were performed with three different amplitudes. In addition, LPC (single 'dip' with $45°$ slopes) was also employed with a phase sweep, different amplitudes and different sign. The most promising noise reductions were identified in the same manner as the maximum BVI condition during the sweep of angle of attack, but now the minimum BVI was searched for. From all the variations, the following conditions were found most promising for a minimum BVI noise radiation: 2/rev HHC with an amplitude of $\Theta_2 = 1°$ and a phase setting of $\varphi_2 = 270°$ and also LPC with a pitch increase of $\Delta\vartheta_{LPC} = 0.75°$ at $\varphi_{dip} = 140°$ rotor azimuth.

For the analysis of array source plots, which show the sources of BVI noise within the rotor plane, the 3rd octave band around $630\ Hz$ was chosen, since at this frequency the highest peak within the narrow-band noise spectrum occurred in the baseline case (see Fig. 15). Fig. 19 shows such array source plots with a dynamic range of $20\ dB$ for the baseline case ($33\ m/s$, $\alpha_S = 7°$) as well as the minimum noise cases for both 2/rev HHC and LPC.
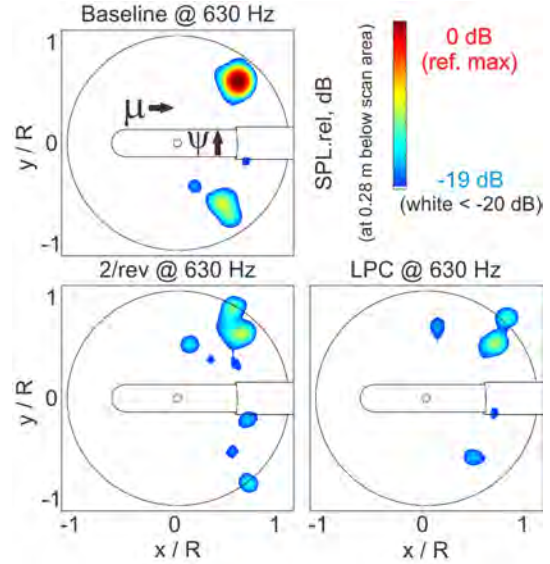

Figure 19: Array source plots for baseline (BL) and minimum noise (MN) cases

Clearly both 2/rev HHC and single dip LPC exhibit significant reductions in this frequency band within the rotor plane – on the advancing side, the intensity is greatly reduced and on the retreating side of the rotor disk the noise source is almost eliminated in both cases. When the respective narrow-band spectra are compared, the differences between minimum noise 2/rev HHC and LPC become more clear. Fig. 20 shows a comparison between the baseline case and minimum noise 2/rev HHC, as well as between both minimum noise cases.

As can be seen in Fig. 20 (top), minimum noise 2/rev HHC significantly reduces noise levels for frequencies $\geq 630\ Hz$ but increases noise for lower frequencies. Compared to the noise levels obtained with the 2/rev HHC input, the minimum noise LPC exhibits lower noise levels over the whole frequency range, see Fig. 20 (bottom).

To maintain comparability of results from the HART and HART II tests [5, 6, 25], the range between the 6th and 40th blade passage frequency ($N_b \cdot \Omega_{ref}$) was chosen for the evaluation of BVI noise levels via noise carpet plots. On a five-bladed rotor system with a nominal rotor speed of $\Omega_{ref} = 110\ rad/s = 17.5\ Hz$, this covers a range from $525\ Hz$ to $3500\ Hz$.

For the baseline case and both minimum noise cases such carpet plots were compiled covering an area of $6\times6\ m$ centered around the rotor hub using data
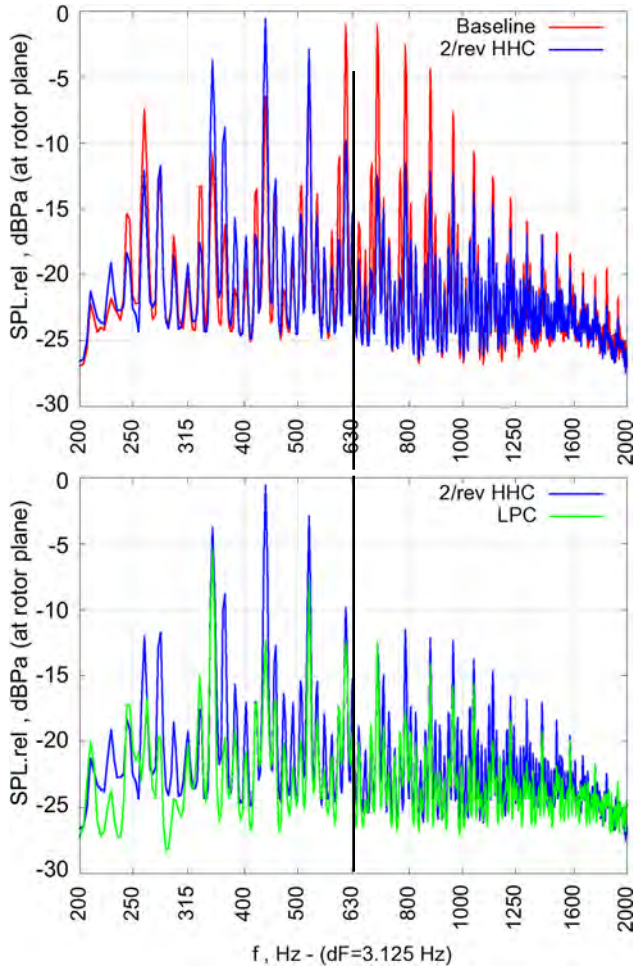
Figure 20: Narrow-band spectra for the baseline case and both MN cases in comparison.

Figure 21: Carpet plots for the baseline case (top), minimum noise 2/rev HHC (bottom left) and minimum noise LPC (bottom right)

from the microphone traverse measurements. Fig. 21 shows all three cases in comparison.

In both minimum noise cases, a significant reduction of the measured noise level is visible, especially on the advancing side of the rotor, where the highest noise levels appeared for the baseline case. For 2/rev HHC (bottom left plot), the peak value on the advancing side of the rotor disk is reduced by $1.5\ dB$ and the area of high-noise emissions is reduced considerably. However, in the fourth quadrant on the retreating side of the rotor disk, noise levels were increased considerably by 2/rev control.

In comparison, the minimum noise LPC input yielded an even higher reduction of BVI noise on the advancing side of the rotor disk (peak value reduced by 3 dB) as well as a slight decrease on the retreating side (fourth quadrant) relative to the baseline. These LPC-results also correspond fairly well with findings from Malovrh et al. [16], where similar inputs in the second quadrant of the rotor disc were found to be highly effective in reducing advancing side BVI noise.

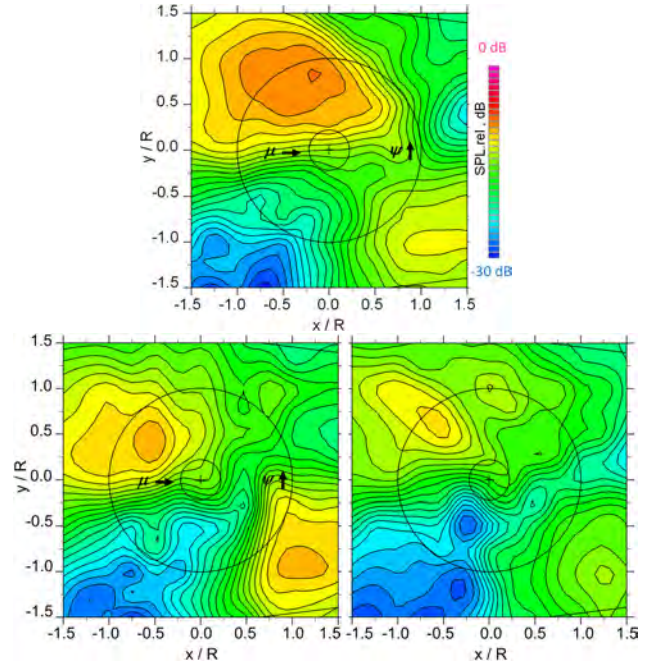It must be noted that due to the asymmetric distribu-

tion of rotor blades among the two swashplates and the resulting multi-harmonic actuator control frequencies (see 'Model rotor and META' section) the control authority for 2/rev (and 3/rev) inputs was severely limited compared to the previous test of the META system on a four-bladed rotor [13]. Therefore it cannot be ruled out that with higher 2/rev control authority ($\Theta_2 > 1.0°$) further reduction of BVI noise could be achieved on the five-bladed rotor.

3.3.3. Pressure measurements for minimum noise HHC and LPC

The physical phenomena leading to a reduction of BVI-noise through 2/rev control and LPC can be understood by a closer look at the blade loading and the high-frequency pressure changes as a result of the blade-vortex interactions. Both control schemes alter the low frequency content of blade aerodynamic loading both radially and azimuthally, and with it the intensity of trailed tip vortex strength. In addition, the distribution of induced velocities within the rotor disk will be modified accordingly, which in return strongly affects the tip vortex trajectory when travelling across the rotor disk. The third physical consequence is a modified blade dynamic response due to the change of airloads mainly in flap and torsion. All together result in a different blade-vortex separation distance at azimuth locations critical for noise radiation. The resulting noise intensity can be amplified or reduced, depending on the HHC or LPC parameters, and those

parameters for a minimum of BVI noise radiation were identified.

In the low frequency (0-9/rev) pressure time histories corresponding to the baseline case and the two minimum noise cases, shown in Fig. 22, it can be seen that the 2/rev control (middle) causes an increase of loading at $\psi = 135°$ and at $315°$, where the blade pitch has the maximum 2/rev upwards deflection, as well as a reduction of loading at $\psi = 45°$ and $225°$, where it is minimum.
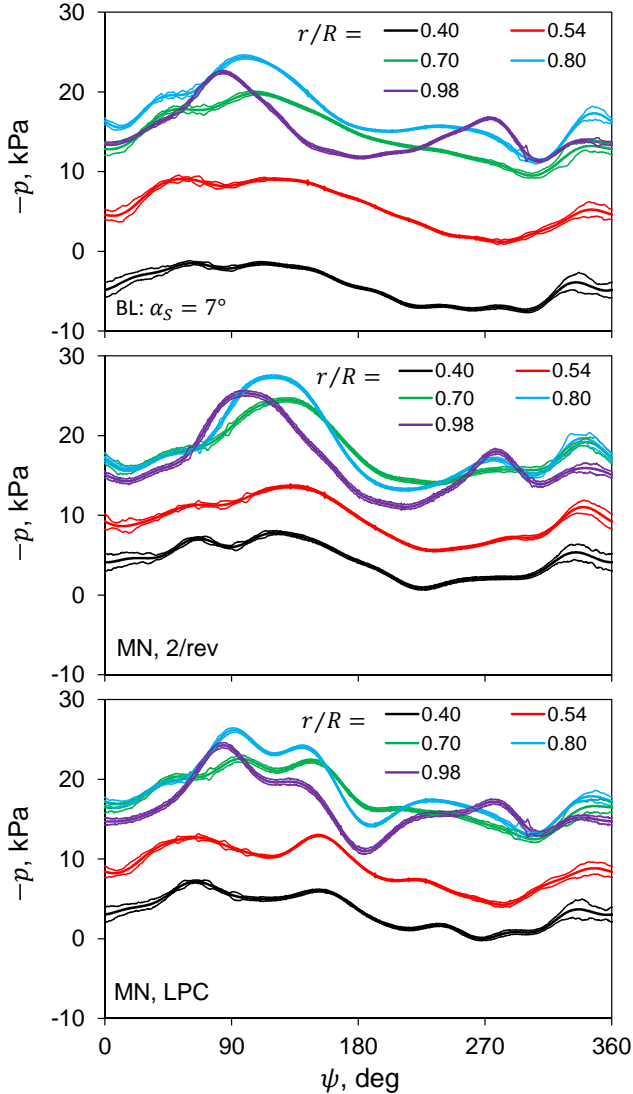

Figure 22: Low frequency pressure signals for BL and MN cases, 0-9/rev, advancing side, $33\ m/s$, $\alpha_S = 7°$.

LPC acts only within a limited range of azimuth, but the blade dynamic response to that excitation extends for a longer range of the rotor revolution (until post-pulse oscillations die out). In Fig. 22 (bottom) the loading exhibits an extra hump relative to the base-line case at the azimuthal position of $\psi = 140°$, and the torsion response following that persists almost un-

til the end of the revolution. The thin lines around the thicker ones indicate the range of standard deviation of local unfiltered pressure data, computed from 32 successive revolutions measured. The time deriva-tives for the most BVI-relevant azimuthal regions in comparison to the BL cases are given in Fig. 23 and Fig. 24.
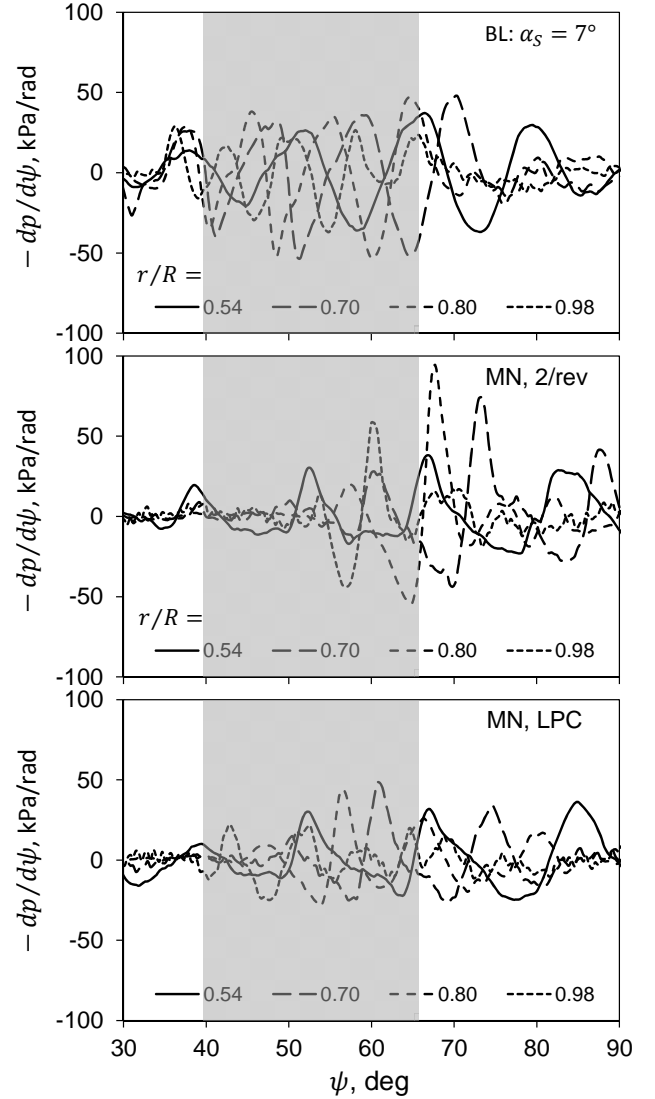

Figure 23: Time derivative of pressure signals for BL and MN cases, h.p. filtered at 10/rev, ad-vancing side, $33\ m/s$, $\alpha_S = 7°$.

The 2/rev control reduces the BVI intensity on both the advancing and the retreating side, see Fig. 23 (middle) and Fig. 24 (middle), each one com-pared to the BL case (top). The physics behind are an increased blade lift in the second quadrant of the disk, which results in an increased downwash in that region, causing the tip vortices to more quickly con-vect downwards than in the BL case and to increase the blade-vortex miss-distance in the first quadrant. On the retreating side the opposite is happening: the reduced blade lift in the third quadrant gener-
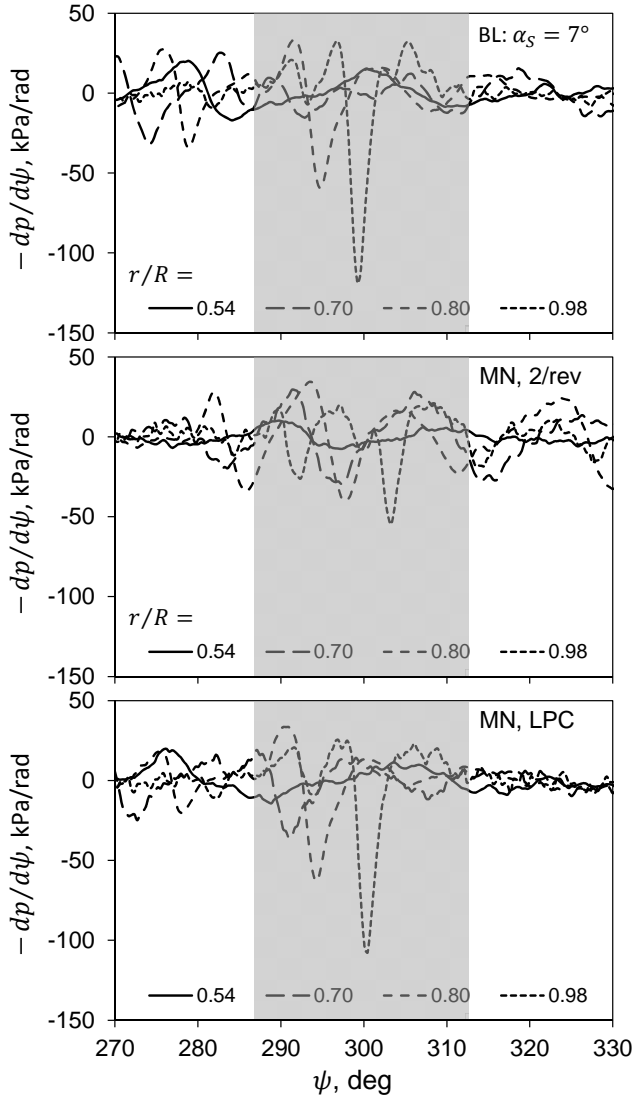
Figure 24: Time derivative of pressure signals for BL and MN cases, h.p. filtered at 10/rev, retreating side, $33\ m/s$, $\alpha_S = 7°$.

Figure 25: BVI in pressure signals for BL and MN cases, h.p. filtered at 10/rev, $33\ m/s$, $\alpha_S = 7°$.

ates weaker vortices than in the BL case and less induced inflow due to less lift, causing tip vortices to a slower downwards convection and to interact with rotor blades later in the fourth quadrant.

Any HHC input changes the blades' pitch all around the revolution, while LPC is affecting only a small azimuthal range without any control outside. Only elastic blade response to it will persist for some successive fraction of the revolution. Therefore the major effect on the advancing side of the disk is about the same as for the 2/rev HHC with the same physics behind, while the retreating side appears only marginal affected relative to the BL case. LPC results are given in the bottom plots of the respective figures, to be compared to the BL case (top).

Fig. 25 shows the pressure fluctuations in a more qualitative form with the contours in the rotor disk.
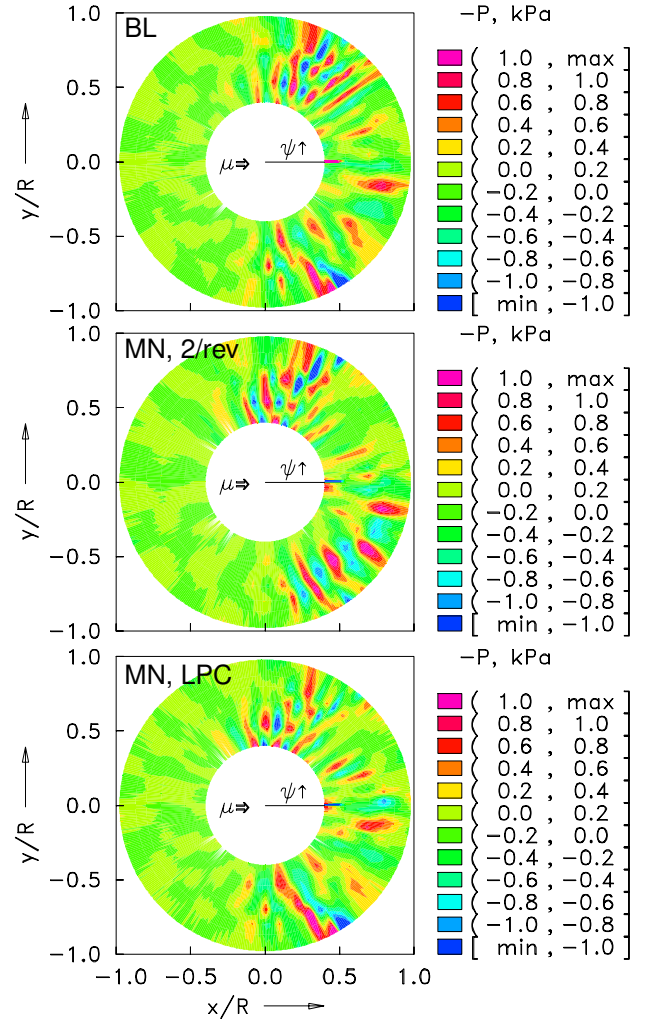
The baseline case (upper graph) clearly shows several strong BVI on the advancing side ($40° \leq \psi \leq 65°$). On the retreating side one strong BVI appears at the blade tip at $\psi = 300°$, plus several more inboard BVI in the range $280 \leq \psi \leq 315°$. A 2/rev minimum noise HHC (middle graph) shifts the advancing side BVI to more upstream locations ($60 \leq \psi \leq 80°$) outside the range of blade-parallel BVI, thus reducing BVI noise. The strong BVI at the blade tip on the retreating side is almost eliminated, while the BVI intensity more inboard of the blade appears increased relative to the baseline case. However, these are confined to a small radial extension, and at these locations the Mach numbers are smaller than at the tip. Finally, the LPC for minimum noise (bottom graph) shows modifications of BVI on the advancing side similar to those of the 2/rev HHC, but with less remaining BVI intensity. The retreating side BVI of the LPC control appears similar to the baseline case, but the inboard BVI appear to be shifted upstream to $\psi = 285°$, al-

most eliminating the BVI following it. The presented analysis of blade pressure measurements thus confirms the results gathered from both microphone array (source plots, Fig. 19) and traverse measurements (Fig. 21).

3.4. Blade deformations

To localize the rotor hub center position and for measuring model movements the circular hub fairing was equipped with 11 SPR markers of $20\ mm$ diameter (Fig. 5). By using these hub markers it was possible to determine the rotor hub center location as well as the current azimuth position of the rotor for calculation of the lead-lag motion of the rotor blades and to determine the model roll and pitch angle. Measurements were done with azimuth increments of $\Delta\psi = 12°$, respectively 30 azimuth positions per revolution such that the analysis allows to synthesize the lower harmonics from 0-6/rev from the time history of the blade motion with good confidence. On every azimuthal position 5 images were taken for averaging purposes in order to get smooth data with reduced errors and eliminated non-harmonic vibrations.

The calculation of the blade motion parameters for flap and lead-lag was be done using the quarter chord line of the rotor blade as described in [26] and [27]. The elastic blade lead-lag deflection y_{el} is given by the distance between the radial position of the quarter chord line and a straight line defined by the current azimuth position of the blade (lag positive). The elastic blade flap deflection z_{el} (positive up) is given by the distance between the quarter chord line and a straight line defined by the pre-cone angle of the rotor head ($\beta_{PC} = 1.85°$). The elastic pitch deformation (θ_{el}, positive nose up) can be calculated by the distance between the z-coordinates of the front and rear blade marker, the associated pitch control angle, the pre-twist angle and the pitch offset in z-direction due to the different distance of the front and rear blade markers to the quarter chord line.

3.4.1. Validation of SPR pitch measurements

The blade root was equipped with two SPR markers to measure the blade pitch angle at the innermost radius at $r/R = 0.1$ without blade torsion. Since the potentiometer based sensors for blade pitch angle measurement are mounted in the same location, a direct comparison between the two sensor systems / approaches was made to test and validate the results computed from the SPR pitch measurements. An example is given in Fig. 26 for the minimum noise LPC control input in descent flight with an amplitude of $\Theta_{dip} = 0.75°$ at an azimuthal location of $\varphi_{dip} = 140°$.

The collective and cyclic pitch control angles are subtracted. The comparison shows a remarkable congruence between the SPR results and the pitch angle sensor(s). Both amplitude and phase angle match very well confirming the high accuracy of the SPR system.
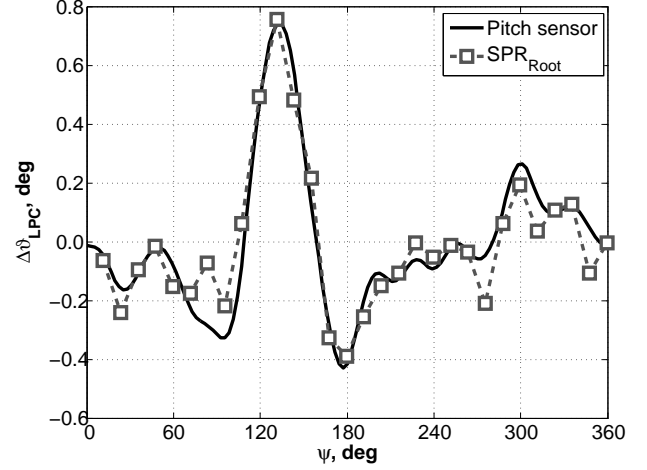

Figure 26: Comparison of measured pitch angle for Dip1 (control angle subtracted)

3.4.2. Hover results

Since in the FTK-META and SKAT wind tunnel tests the same blade loading and identical blades were used, a comparison of a hover thrust sweep can be made. Thrust sweeps were performed between $0N$ and $7000\ N$ in FTK-META and between $-1500\ N$ and $7700\ N$ in SKAT. In Fig. 27 the elastic tip deflection in lag (averaged over all rotor blades) is given for both rotors. For $C_T/\sigma < 0.05$ the blade tips are in a lead position (partly due to a built-in pre-lead angle), above $C_T/\sigma = 0.05$ the blades are in lag position.
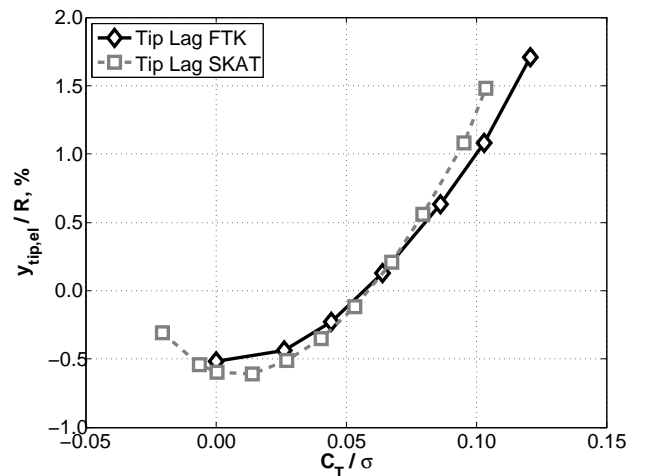

Figure 27: Comparison of elastic blade tip lag displacement

The comparison of the elastic blade tip deflection in flap direction is shown in Fig. 28. The gradient of both curves is very similar but an offset of about 12 mm can be found for the SKAT test compared to the flap displacement measured during the FTK-test. This offset results from the different pre-cone angles of both rotor heads ($\beta_{pc,FTK} = 2.5°$, $\beta_{pc,SKAT} = 1.85°$).
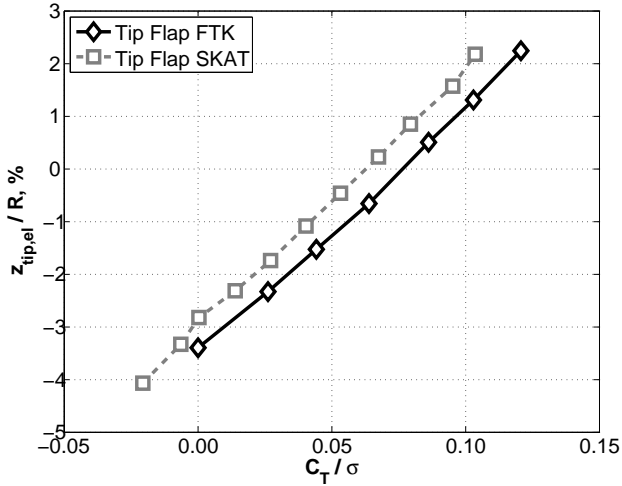

Figure 28: Comparison of elastic flap displacement at the blade tip

3.4.3. HHC results

During the SKAT test HHC inputs with frequencies from 2/rev to 6/rev were executed. The results of n/rev SPR measurements for the descent flight condition ($\mu = 0.15$) are presented in Fig. 29.
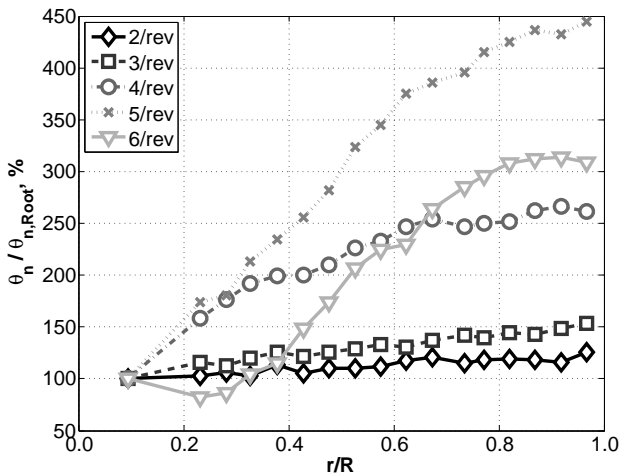

Figure 29: n/rev pitch amplitudes versus blade radius

The changes in n/rev amplitude are plotted oder the blade radius relative to the amplitude of the control input at the blade root. In all n/rev cases the control input amplitude is amplified with increasing blade radius

up to the tip ranging from 125% for 2/rev input up to 450% for 5/rev HHC. Since the first torsion frequency of the FTK blades is about 4.7/rev, the maximum amplitude amplification can be found for 4/rev and 5/rev control. The maximum phase delay was found for the 6/rev input at $\Delta\varphi_6 \approx 135°$, as shown in Fig. 30 for all n/rev HHC inputs.
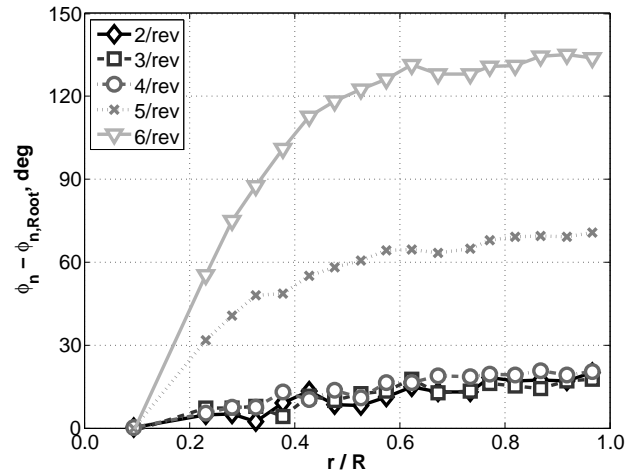

Figure 30: n/rev pitch phases versus blade radius

4. Conclusions

Following earlier wind tunnel tests with 4 rotor blades [13] and as part of a joint research project with Airbus Helicopters Germany, the DLR's Multiple Swashplate System was modified for 5-bladed IBC operation and tested in the Large Low-Speed Facility of the DNW. During those tests, several different IBC strategies were employed to increase rotor performance and to reduce vibration levels and noise emissions. The main conclusions of the test are:

- Using 2/rev HHC with an amplitude of $\Theta_2 = 1.0°$ the required rotor power in high-speed flight condition ($\mu = 0.345$) was reduced by a maximum of 5.6% compared to the baseline case. The optimum 2/rev phase of $\varphi_2 = 240°$ corresponds well with results from earlier 4-bladed wind tunnel tests.

- In high-speed flight ($\mu = 0.345$) 3/rev control yielded a maximum power reduction of $\Delta P_{eff} = -2.8\%$ with an amplitude of $\Theta_3 = 0.8°$ and an optimum phase setting of $\varphi_3 = 0°$.

- The optimum 3/rev HHC settings for performance enhancement in high-speed flight also yielded the lowest 5/rev vibration instrusion index VI_5, which was reduced to 40% of its baseline value. Thus, 3/rev HHC shows potential to reduce both required rotor power and vibration simultaneously on a 5-bladed, hingeless rotor system.

- Due to the actuators of the META system exerting 5/rev forces on the rotor balance during 4-6/rev IBC operation, similar reductions of vibrational hub loads could not be measured for these control frequencies. However, the analysis of blade bending moments indicates that significant vibration reductions can be achieved with 4-6/rev IBC on a five-bladed rotor.

- A T-matrix based vibration controller was adapted for operation on a five-bladed rotor system and its effectiveness successfully demonstrated in the wind tunnel. However, the reduction of the weighted vibration intrusion index VI_5 by 83% in high speed flight ($\mu = 0.345$), was mostly a result of 5/rev actuator forces counteracting the 5/rev vibrational loads measured by the rotor balance.

- The maximum BVI-case in descent flight ($\mu = 0.15$) was found for a shaft angle of $\alpha_S = 7°$ using measurements from the DNW's microphone array and confirmed by on-blade pressure measurements. This shaft angle setting was used as baseline case for further noise investigations.

- Both 2/rev HHC and LPC were effectively used to reduce BVI-noise levels in simulated descent flight at $33\ m/s$ ($\mu = 0.15$).

- In the frequency range of 6-40th BPF, which was used to ensure comparability with the earlier HART and HART II tests, single-'dip' LPC yielded significantly higher noise reductions than 2/rev HHC. High-noise areas were reduced considerably in both size and magnitude, with a reduction in peak SPL of $3.0\ dB$.

- Pressure measurements both confirmed the results from the acoustic measurements and served to identify changes in tip-vortex strength and vortex trajectories as the physical phaenomena resulting in BVI-noise reductions.

- Using the proven and enhanced SPR system of DNW-LLF, the blade motion of all five rotor blades as well as the model pitch and roll angles were analyzed. A comparison of the SPR results with the conventionally measured blade pitch angles shows very good congruence.

Supported by:

Federal Ministry
for Economic Affairs
and Energy

on the basis of a decision
by the German Bundestag

References

[1] C. Kessler, "Active Rotor Control for Helicopters: Motivation and Survey on Higher Harmonic Control," *CEAS Aeronautical Journal*, vol. 1, no. 1-4, pp. 3–22(20), 2011.

[2] C. Kessler, "Active Rotor Control for Helicopters: Individual Blade Control and Swashplateless Rotor Designs," *CEAS Aeronautical Journal*, vol. 1, no. 1-4, pp. 23–54(22), 2011.

[3] P. P. Friedmann, "On-blade control of rotor vibration, noise, and performance: Just around the corner?," *Journal of the American Helicopter Society*, vol. 4, no. 59, pp. 1–37(37), 2014.

[4] Y. H. Yu, B. Gmelin, H. Heller, J. J. Philippe, E. Mercker, and J. S. Preisser, "HHC Aeroacoustics Rotor Test at the DNW - The Joint German / French / US HART Project," in *20th European Rotorcraft Forum*, (Amsterdam, The Netherlands), Oct. 4-7, 1994.

[5] W. R. Splettstoesser, R. Kube, W. Wagner, U. Seelhorst, A. Boutier, F. Micheli, E. Mercker, and K. Pengel, "Key Results From a Higher Harmonic Control Aeroacoustic Rotor Test (HART)," *Journal of the American Helicopter Society*, vol. 42, no. 1, pp. 58–78(21), 1997.

[6] B. G. van der Wall, B. Junker, C. L. Burley, T. F. Brooks, Y. H. Yu, C. Tung, M. Raffel, H. Richard, W. Wagner, E. Mercker, K. Pengel, H. Holthusen, P. Beaumier, and Y. Delrieux, "The HART II Test in the LLF of the DNW - a major step towards rotor wake understanding," in *28th European Rotorcraft Forum*, (Bristol, UK), Sept. 17-20, 2002.

[7] B. G. van der Wall, J. W. Lim, M. J. Smith, S. N. Jung, J. Bailly, J. D. Baeder, and D. D. Boyd, "The HART II International Workshop: An Assessment of the State-of-the-Art in Comprehensive Code Prediction," *CEAS Aeronautical Journal*, vol. 4, no. 3, pp. 223–252(30), 2013.

[8] B. G. van der Wall and R. Bartels, "Patent für eine Hubschrauber-Rotorsteuereinrichtung."

Pat.-Nr.: DE-10-2006-030-089-D, Deutsches Patent- und Markenamt, Jan. 2008.

[9] P. Küfmann, "Patent für ein Verfahren zum Ermitteln von Stellgrößen." Pat.-Nr.: DE-10-2010-024-089-B4, Deutsches Patent- und Markenamt, Jan. 2013.

[10] R. Bartels, P. Küfmann, and C. Kessler, "Novel Concept for Realizing Individual Blade Control (IBC) for Helicopters," in *36th European Rotorcraft Forum*, (Paris, Frankreich), Sept. 7-9, 2010.

[11] P. Küfmann, R. Bartels, C. Kessler, and B. G. van der Wall, "On the Design and Development of a Multiple-Swashplate Control System for the Realization of Individual Blade Control for Helicopters," in *67th Annual Forum of the American Helicopter Society*, (Virginia Beach, VA, U.S.A.), May 3-5, 2011.

[12] P. Küfmann, R. Bartels, and O. Schneider, "DLR's Multiple Swashplate Control System: Operation and Preliminary Testing," in *38th European Rotorcraft Forum*, (Amsterdam, The Netherlands), Sept. 4-7, 2012.

[13] P. Küfmann, R. Bartels, B. G. van der Wall, O. Schneider, H. Holthusen, J. Gomes, and J. Postma, "The First Wind-Tunnel Test of the DLR 's Multiple Swashplate System : Test Procedure and Preliminary Results," in *72nd Annual Forum of the American Helicopter Society*, (West Palm Beach, FL, U.S.A.), May 17-19, 2016.

[14] P. Küfmann, R. Bartels, B. G. van der Wall, O. Schneider, H. Holthusen, J. Gomes, and J. Postma, "The First Wind Tunnel Test of the Multiple Swashplate System: Test Procedure and Principal Results," *Journal of the American Helicopter Society*, accepted for publication May 4th 2017.

[15] P. Küfmann and C. Brillante, "Implementation and Test of a Semi-Closed Loop HHC-Algorithm with the DLR's Multiple Swashplate System," in *41st European Rotorcraft Forum*, (Munich, Germany), Sept. 1-4, 2015.

[16] B. Malovrh and F. Gandhi, "Localized Individual Blade Root Pitch Control for Helicopter Blade-Vortex Interaction Noise Reduction," *Journal of the American Helicopter Society*, vol. 55, no. 3, pp. 032007–1–032007–12(12), 2010.

[17] F. Kody, E. Corle, M. D. Maughmer, and S. Schmitz, "Non-Harmonic Deployment of Trailing-Edge Flaps for Rotor-Performance Enhancement and Vibration Reduction," in *5th Decennial AHS Aeromechanics Specialists' Conference*, (San Francisco, CA, U.S.A.), American Helicopter Society Inc., Jan. 22-24, 2014.

[18] P. Küfmann, R. Bartels, and B. G. Wall, "Localized Blade-Root IBC for Rotor-Performance Enhancement and Vibration Reduction," in *40th European Rotorcraft Forum*, (Southampton, UK), Sept. 2-5, 2014.

[19] F. Kody, E. Corle, M. D. Maughmer, and S. Schmitz, "Higher-Harmonic Deployment of Trailing-Edge Flaps for Rotor-Performance Enhancement and Vibration Reduction," *Journal of Aircraft*, vol. 53, no. 2, pp. 1–10(11), 2015.

[20] P. Küfmann, R. Bartels, and B. G. van der Wall, "Rotor performance enhancement via localized pitch control and its effects on hub vibrations and pitch link loads," *CEAS Aeronautical Journal*, vol. 8, no. 1, pp. 181–196(16), 2017.

[21] S. Crews and B. Hamilton, "Army helicopter crew seat vibration – past performance, future requirements," in *American Helicopter Society North East Region National Specialists' Meeting on Helicopter Vibration*, November 1981.

[22] AMCOM, "ADS-27A-SP - requirements for rotorcraft vibration specifications, modeling and testing," 2006.

[23] W. Johnson, "Self-Tuning Regulators for Multicyclic Control of Helicopter Vibration," NASA Technical Paper TP-1996 (A-8719), Scientific and Technical Information Branch, Moffett Field, CA, U.S.A., March 1982.

[24] R. M. Morales, M. C. Turner, P. Court, and C. Hutchin, "Actuator Constraints Handling in Higher Harmonic Control Algorithms for Vibration Reduction," in *Proceedings of the 40th European Rotorcraft Forum*, (Southampton, UK), Sept. 2-5, 2014.

[25] W. R. Splettstoesser, K.-J. Schultz, R. Kube, T. F. Brooks, E. Booth, G. Niesl, and O. Streby, "A Higher Harmonic Control Test in the DNW to Reduce Impulsive BVI Noise," *Journal of the American Helicopter Society*, vol. 39, no. 4, pp. 3–13(11), 1994.

[26] O. Schneider, B. G. van der Wall, and K. Pengel, "HART II Blade Motion Measured by Stereo Pattern Recognition (SPR)," in *Proceedings of the 59th Annual Forum of the American Helicopter Society*, (Phoenix, AZ, U.S.A.), May 6-8, 2003.

[27] O. Schneider, "Analysis of SPR measurements from HART II," *Aerospace Science and Technology*, vol. 9, no. 5, pp. 409–420(12), 2005.